March - April 2020
ISSN: 0193-4120 Page No. 202 - 215

Image Processing Techniques in Automatic Diabetic Retinopathy Screening Systems

V. Sivakumar1 and Muhammad Akbar Husnoo2

[1, 2]School of Computing, Asia Pacific University of Technology and Innovation (APU),

Bukit Jalil, Malaysia-57000

1dr.sivakumar@apu.edu.my, [2]muhammad.akbar.husnoo@hotmail.com

Article Info
Volume 83
Page Number: 202 - 215
Publication Issue:
March - April 2020

Article History

***Article Received**: 24 July 2019*
***Revised**: 12 September 2019*
***Accepted**: 15 February 2020*
***Publication**: 12 March 2020*

Abstract

With the increased number of people suffering from diabetes, there is an urgency to automate Diabetic Retinopathy Detection. According to the International Diabetic Federation, there are over 93 millions of patients suffering from Diabetic Retinopathy world-wide. Currently, there are three types of manual screening procedures to detect Diabetic Retinopathy which include Pupil Dilation, Ophthalmoscopy and Tonometry. Several attempts to automate the screening of Diabetic Retinopathy has been made over the last two decades. An Automatic Diabetic Retinopathy Screening System (ADRSS) serves as a supporting tool for an Ophthalmologist to increase the speed and accuracy of Diabetic Retinopathy Detection. In the domain of research, several such systems have been made available which makes use of ocular images different imaging modalities. Depending upon different modalities, different image processing algorithms have been put in practice. In this juncture, this proposed aims to study and analyze all the different detection techniques available with an emphasis to techniques for respective image modalities. This proposed paper will conduct a detailed review on the different algorithms that are being implemented of the different types of images from different modalities with their diagnostic level of accuracy in Diabetic Retinopathy Screening.

Keywords: *Automatic Diabetic Retinopathy Screening System, imaging modalities, ocular images.*

1. Introduction

According to Diabetic Retinopathy Barometer, a study carried out by the International Diabetes Federation in conjunction with the International Federation on Ageing & the International Agency for the Prevention of Blindness in 41 countries, there are around 93 million people worldwide which are reported to be living with DR while the actual figure might sky-rocket further if including unreported ones[1].

Globally, diabetes is a chronic ailment that is affecting millions of people. Diabetes is the mother of all diseases[2]. It leads to several other health complications. Once such complication is Diabetic Retinopathy.

Diabetic Retinopathy (**DR**) is an ocular disorder suffered by diabetic patients if their blood glucose level is not closely monitored and controlled. It is globally posing a current health threat to the middle-age population in developed nations such as the United States, whereby the number of cases rose to 4.06 to 7.69 million within less than a decade[3].

High levels of sugar in the diabetic patient's blood leads to the blockage of retinal blood vessels causing them to swell, explode and leak blood into the retina. This disorder advances progressively

March - April 2020
ISSN: 0193-4120 Page No. 202 - 215

from an early reversible stage to causing visual impairments, lessening visual acuity, blurring vision and eventually to the irreversible total blindness of the patient[4].

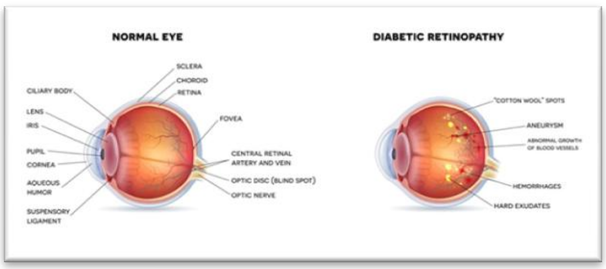

Figure 1: Normal Person's Eye V/S Dr Patient's Eye.

However, according to the Diabetic Retinopathy Barometer (previously mentioned), 21 % of ophthalmologists were not given the proper training or do not know how to diagnose DR at the proliferative stage.This occurs due to the lack of symptoms during the early stage of DR. In most cases, the symptoms usually occur during the irreversible stages until the patient suffers from sudden loss of vision or visual problems. 1 out of 3 diabetic patients are prawn to develop retinopathy over their lifetime[1].

Moreover, due to the swift increasing rate of diabetic patients, ophthalmologists are not able to screen the massive number of retinal fundus images manually at a high response rate. According to the International Council of Ophthalmology, the total number of ophthalmologists is around 200,000 to 300,000 worldwide and a shortfall is expected to occur in the near future[5].

The lack of ocular specialists is critical, and the short number is unable to manage this enormous number of diabetic patients. By simple estimated calculation, one (1) ophthalmologist must screen around 1400 retinal images at a time. This shows that there is a lack of manpower needed to control and regulate this ailment. 38 % of the patients often say that long waiting times were a major barrier that made them refrain from regular eye check-ups. Mass manual screening takes a rather longer period of time and the patients have to wait a longer time period in order to do an eye check-up.

Furthermore, in agreement with CTV News, poverty can twofold or even threefold the likelihood of being a diabetic patient[6]. The scarcity of ophthalmologists makes check-ups expensive. Manual screening, along with its precise diagnostic results, has a short-coming. Manual screening of DR tends to be costly and beyond the financial capability of the average lower-class family. In Scotland alone, after a study was conducted, as mentioned by Ophthalmology Times, manual screening of DR proved to be £ 200,000 costlier and the same amount was saved after the implementation of automatic screening.

2. Ocular Imaging Modalities

According to Khaderi et al., Hermann von Helmholtz invented the first direct ophthalmoscope in 1851 while Novotny and Davis invented Fluorescein Angiography (**FA**) in 1961. This FA led to another discovery known as Fundus Autofluorescence (**FAF**). In the 1990's, Optical Coherence Tomography (**OCT**), a non-invasive technique was detected which is commonly in clinical practice nowadays. These are several types of OCT such as Time-Domain OCT, Spectral-Domain OCT and Frequency-DomainOCT which makes use of Fourier Transformation. Moreover, there are two ways to acquire fundus ocular images.

In line with the research carried out by Saeed and Oleszczuk, there are several Ocular imaging techniques that have been constantly evolving starting from indirect ophthalmoscope, direct ophthalmoscope, slit lamp with different lenses, Fundus Fluorescein Angiography (**FFA**), Fundus Photography, 3-D Photography, confocal scanning laser ophthalmoscope (**cSLO**) and OCT.

Previously, film-based retinal photography was a major contributor. However, with the fast-paced advent of new technologies, the usage of digital auto-focus and infrared focus cameras and systems in telemedicine has revolutionized the way retinal images are captured. Some of the approved cameras

TEST Engineering & Management

March - April 2020
ISSN: 0193-4120 Page No. 202 - 215

are Topcon NW8, Zeiss Cirrus 600, etc. They also stated that there are two types of cameras:

- **Non-Mydriatic Fundus Cameras**: Does not require pupil dilation and makes use of retina's reflective properties to show details and store images.
- **Mydriatic Fundus Cameras:** Requires pupil dilation which may be painful for a patient.

Color fundus photos are usually taken using mydriatic cameras due to the requirement of pupil dilation. The researchers have stated that images that were obtained without pupil dilation were of poor quality compared to pictures that were taken using pupil dilation[7].

Moreover, there are new automatic retinal imaging systems such as DRS that senses the eyes, automatically aligns and focuses on the pupil and retina to take the image which significantly reduces human effort.

3. Developments in Automatic Diabetic Retinopathy Screening Systems

According to Gardner et al., their research made use of an AI neural network for screening Diabetic Retinopathy. The researchers created back propagation neural network using Neural Works Professional II/Plus. They used a digital mydriatic camera (Canon Fundus – 60UV) to capture 147 ocular images of patients suffering from DR and 32 ocular images from normal person. Those ocular images then underwent a scanning process using "Nikon Coolscan" to provide images of uniform pixel size (700 x 700) and were then further devised into smaller squares of 30 x 30 and 20 x 20 pixels using a program that was specifically written in C language for that purpose. The photographs were pre-processed to remove the red wavelength from the images. The images were grouped by categories, e.g., normal retina, damaged retina, hemorrhages, etc. Those images were then fed to the neural network as training data. Once the neural network was ready after training, the accuracy of the system was compared to that of a manual screening by an ophthalmologist. 200 DR images and 101 normal images were randomly given to the eye specialist for screening. The accuracy rate was 83.5%. The neural network was not able to screen for DR on low contrast images[8].

The work done by Sinthanayothin et al., included the practice of a new image processing technique known as Moat Operator. The researchers utilized a non-mydriatic camera (Topcon TRC-NW 5S) to capture digital fundus ocular images that were stored in tiff format. The RGB images obtained were converted into HIS images whereby Adaptive and Local Contrast Enhancement method were applied. A multilayer perceptron neural network using Principle Component Analysis was utilized for the recognition of OD and blood vessels. The pictures were then adjusted to a red-orange standard. A recursive region growing segmentation (RRGS) algorithm was utilized for exudate detection. The OD was extracted using Position Recognition Algorithm. Moat Operator was applied for sharpening edges of red lesions. The sensitivity and specificity for exudate detection were 88.5% and 99.7% respectively. Hard Exudate detection sensitivity and specificity was 77.5 and 88.7 % respectively[9].

line with the research done by Sopharak et al., their research made use of mathematical morphology methods for screening Diabetic Retinopathy. The researchers used a non-mydriatic camera (KOWA - 7) to capture digital fundus ocular images that were stored in JPEG format with minimum image compression. The images were preprocessed by firstly converting them into HIS images and applying a Median Filtering Operation to reduce noises. Contrast-Limited Adaptive Histogram Equalization (CLAHE) was used for contrast enhancement. To eliminate the Optical disc, grayscale closing operator was applied and image thresholding technique was applied. Morphological dilation was applied to reconstruct the image and the optic disc was masked out. A closing operator was again applied for eliminating blood vessels and a local variation operator was applied for exudate detection. 60 images were tested and compared with the results of an ophthalmologist. The sensitivity

March - April 2020
ISSN: 0193-4120 Page No. 202 - 215

and specificity of the system by use of morphology methods were 80 % and 99.5 % respectively[10].

Additional research carried out by Sopharak et al., their research made use of Fuzzy C-means clustering for screening Diabetic Retinopathy. The researchers used a non-mydriatic camera (KOWA - 7) to capture digital fundus ocular images that were stored in JPEG format with minimum compression. The RGB images were firstly converted in HSI images and CLAHE was used for preprocessing. The standard deviation of intensity of the image after CLAHE was measured. Sobel Edge Operator with a masking size of 3 x 3 was used for edge detection. Decorrelation stretching, Contrast exaggeration and thresholding was used for detection of blood vessels. Local Entropy, Otsu's Algorithm and binary dilation was used for identification of the OD. Fuzzy C-Mean clustering was used to detect exudates. Morphological reconstruction based on neighboring pixels was used for a more refined segmentation. The accuracy of using a combination of Fuzzy C-Mean clustering and morphological reconstruction was around 99% for 40 images that were tested[11].

4. Overview of the most commonly used algorithms

4.1.Histogram Equalization

Histogram Equalization is a largelyutilized technique in many fields such as medical image processing, spatial image processing, and so on, for adjusting image intensities to enhance contrast.

There is a common misconception relating to histogram equalization. During histogram equalization, the contrast of an image is enhanced. This does NOT mean that the contrast is always increased. There are cases where the contrast is also decreased[12.]

There are two types of Histogram Equalization as shown in the following:

4.1.1. Local Histogram Equalization

According to the University of Utah, the histogram of an image is a distribution of its discrete intensity levels in the range [0, L-1].

During Local Histogram Equalization. there is a redistribution of pixel values to give a linear trend to the cumulative distribution probability of the image[13].

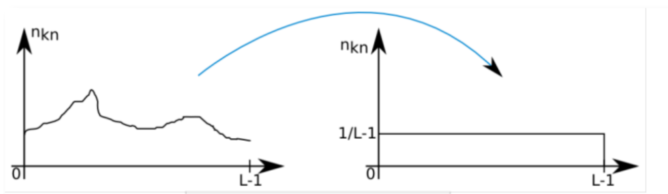

Figure 2: Linear Distribution of Gray Pixels After Histogram Equalization

In the above figure, there are two graphs. The first graph is the Intensity histogram of a grey-level representation of a random image before pre-processing. It can be seen from the first graph that the pixels have been unevenly distributed across the image whereby there are regions with high densities of gray pixels and regions with low densities of gray pixels. On the second graph, after having processed the image with Local histogram equalization, there is an equal distribution of the gray pixels across the image. [13][14]

This idea that has been explained so far is a mathematical concept making use of the **Cumulative Distribution function** (cdf). The cdf is cumulative sum of all the probabilities in a certain domain range. The main mathematical formula relating to histogram equalization is shown below:

$$cdf(x) = \sum_{k=-\infty}^{x} P(k)$$

Figure 3: Local Histogram Equalization Mathematical Representation

[14]

The effect of applying Local Histogram Equalization technique on a particular image can be

March - April 2020
ISSN: 0193-4120 Page No. 202 - 215

seen on the two pictures shown on the following page.

[4] *[5]*

Figure 4: Original Image , **Figure 5**:After Applying Local Histogram Equalization

From the two figures above showing the effect of applying Local Histogram Equalization technique, it can be deduced that local Histogram Equalization carries some negative effects on the image:

- The mean brightness of the image lies in the middle of the image;
- Enhancement of the borders and the edges rather than the inner part of the image;
- Over Enhancement of the edges, resulting in stretching and distortion of the edges; &
- Creates additional noise in the image.

4.1.2. Adaptive Histogram Equalization

Usually, the distribution of gray pixels in an image is not distributed similarly across an image. The AHE is another method of Histogram Equalization used for contrast enhancement of an image. AHE is different from Local Histogram Equalization in the sense that it computes various histograms for each and every section on an image before remapping the pixel in the most effective and efficient way. [15]

In AHE, each pixel is adjusted using a transformation function based on the pixel that is in the surrounding/neighbouring region of that pixel. In a more technical term, each pixel is adjusted from the Cumulative Distribution Function (refer to Local Histogram Equalization) of the pixel values of the contextual region. [15]

[6] *[7]*

Figure 6: Original Image, **Figure 7:** After Adaptive Histogram Equalization

From the two images, it can be deduced that AHE has some positive effects on an image:

- As the name suggest, AHE is an adaptive method as the results are not affected by the uneven distribution of pixel values across an image; &
- Produces superior images that the Local Histogram Equalization Technique.

[16]

However, AHE brings along a drawback of not only enhancing the image contrast but also adding more noise to the image or worsening noise of an image. For this concern, an extension of the AHE has been developed. This technique is known as **Contrast-Limited Adaptive Histogram Equalization**. [15]

4.1.3. Contrast Limited Adaptive Histogram Equalization

CLAHE was primarilypioneered for catering the needs & overlapping the constraints of AHE during Medical image Processing. CLAHE, as stated above, is an extension of the normal AHE.

As opposed to AHE, CLAHE works on small segments of the image rather than on the whole image. The image is broken down into small areas

March - April 2020
ISSN: 0193-4120 Page No. 202 - 215

called tiles. The contrast of each tile is improved using Cumulative Distribution Function (refer to Local Histogram Equalization). The neighbouring tiles are later joined together using bilinear interpolation (i.e. in a simple way, addition of x-axis first and y-axis afterwards) to eliminate artificially induced boundaries. [16]

[8] ***[9]***

Figure 8**:** Original Image **, Figure 9:** After Clahe Algorithm Application

Although CLAHE has several advantages such as it prevents the amplification of noise, enhances contrast and produces better results compared to other AHE and LHE, it also has some major drawbacks of its application:

- It is an expensive algorithm to implement for commercial usage;
- It is a very complex algorithm;
- It is time-consuming as there is sequential tile-by-tile enhancement and interpolation.

4.2.Median Non-Linear Filtering

Salt and Pepper noise is a type of impulse noise caused by sharp and sudden disturbances in an image signal affecting the quality of an image. An image containing salt and pepper noise can be easily identified as the image will contain dark pixels in bright regions and bright pixels in dark regions. [17]

An example of an image that has been distorted with salt and pepper noise is shown in the following:

Figure 10: Image Containing Salt & Pepper Noise

To overcome type of impulse noise, **Median Non-Linear Filtering**, a noise reduction algorithm was proposed.

Median Non-Linear Filtering technique runs through an image pixel by pixel and considers the neighbouring pixels of a particular pixel. The neighbouring pixels form a group called a window. After considering the pixel values in the neighbouring pixels, the particular pixel value is replaced with the median of the pixel values of the window. In a more technical way, median Non-Linear Filtering involves masking of a pixel value from its neighbouring pixels. [18]

Since it is quite complicated to grasp from the definition above, the researcher will like to diagrammatically represent this idea for a better clearer explanation as shown in the following.

With all due respect, allow the researcher to consider the highlighted value (150) as the chosen pixel and the chosen pixel value to demonstrate the process of Median Non-Linear Filtering Algorithm.

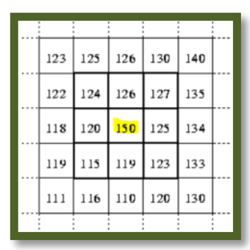

123	125	126	130	140
122	124	126	127	135
118	120	150	125	134
119	115	119	123	133
111	116	110	120	130

Figure 11: Matrix Representation Of Pixel Values In An Image

In this example a 3 X 3 window is used to demonstrate the effect of Median Non-Linear Filtering algorithm Since 150 is the chosen pixel value, the neighbouring pixel values are:

TEST Engineering & Management

March - April 2020
ISSN: 0193-4120 Page No. 202 - 215

124, 120, 115, 119, 123, 125, 127, 126, 150

To calculate the median value, rearrange the list of pixels in ascending order (starting from the smallest pixel):

115, 119, 120,123, 124, 125, 126, 127, 150

Since the median is the middle value of a list of values, 124 is picked as the median value. The pixel value of 150 is finally replaced with the median value of 124.

[19]

An example of applying median non-linear filtering algorithm on an image is shown below:

Figure 12: Before and After Applying Median Non-Linear Filtering

Mathematical Morphology is an image segmentation approach that is makes use of the object size and shape rather than the pixel intensity. It is used for the analysis of shapes and to extract components and is mostly based on set theory. Sets are used to represent objects in an image.

Mathematical morphology has four (**4**) basic operators which are:

4.3.1. Erosion

Erosion is usually applied on binary images. However, there are some variations that are fit for application on gray-scale images. The basic idea of Erosion is to simultaneously **shrink** the number of white pixels and increase the number of black pixels in order to increase holes.

$\ominus$ • Erosion

Figure 13: Erosion Operator

To fully understand the concept of erosion, the researcher has manually represented an image in the form of a matrix as shown in the following figure. The researcher wishes to highlight that 0s represent white pixels and 1s represent white pixels.

$$\begin{pmatrix} 1 & 1 & 1 & 1 \\ 1 & 0 & 0 & 1 \\ 1 & 0 & 0 & 1 \\ 1 & 1 & 1 & 1 \end{pmatrix}$$

Figure 14: Original Image Matrix

The **Structuring Element**, also known as the kernel, is a small set that is used to probe through the image. The kernel shape is adapted based on the geometrical shape of the image. In this situation, the researcher has defined a 2 x 2 kernel which is shown in the following figure:

$$\begin{pmatrix} 1 & 1 \\ 1 & 1 \end{pmatrix}$$

Figure 15: Kernel 2 X 2 Matrix

This kernel is now slid over the image for probing. The basic logic behind this probe is to check if there is a perfect match between the kernel and the image. The result of the probe over each pixel arises to two (**2**) scenarios:

- **Perfect Match:** All the image pixel values matches the all the kernel pixel values at the point where the kernel is being applied. The result of the probe will be 1 assigned to the image pixel.
- **No Match:** One or all the image pixel values do not match the all the kernel pixel values at the point where the kernel is being applied. The result of the probe will be 0 assigned to the image pixel.

The first probe is shown in the picture below. Since the pixel values of the image do not match that of the kernel, the pixel value 1 is changed to pixel value 0.

$$\begin{pmatrix} 0 & 1 & 1 & 1 \\ 1 & 0 & 0 & 1 \\ 1 & 0 & 0 & 1 \\ 1 & 1 & 1 & 1 \end{pmatrix}$$

Figure 16: First Probe + Result

The second probe is shown in the following diagram. Since the pixel values of the image do not match that of the kernel, the pixel value 1 is changed to pixel value 0.

$$\begin{pmatrix} 0 & 1 & 1 & 1 \\ 1 & 0 & 0 & 1 \\ 1 & 0 & 0 & 1 \\ 1 & 1 & 1 & 1 \end{pmatrix}$$

Figure 17: Second Probe + Result

The probing process is iterated through the whole image until the last line of the image matrix is reached. Since there are no values, the probing process is stopped as shown below:

$$\begin{pmatrix} 0 & 0 & 1 & 1 \\ 1 & 0 & 0 & 1 \\ 1 & 0 & 0 & 1 \\ 1 & 1 & 1 & 1 \end{pmatrix}$$

Figure 18: Probing Cannot be Further Continued.

Since the probing process is discontinued at the last line of the image matrix, the last line of the image matrix remains unchanged. Therefore, the final erosion matrix experiences an increase in black pixels and a decrease in white pixel as shown in the following:

$$\begin{pmatrix} 0 & 0 & 0 & 1 \\ 0 & 0 & 0 & 1 \\ 0 & 0 & 0 & 1 \\ 1 & 1 & 1 & 1 \end{pmatrix}$$

Figure 19: Final Image After Erosion

An example of applying erosion on a binary image is shown below:

[20] ***[21]***

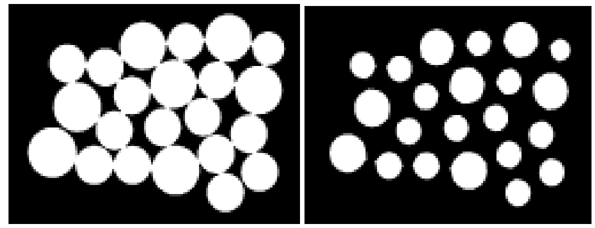

Figure 20: Original Image ,Figure 21: Resulting Image After Applying Erosion

During morphology, an imaged is viewed as a subset of the Euclidean Space. In a more mathematical way of representation, erosion is shown as a formula as shown below:

$$A \ominus B = \{z \in E^2 : (B)_z \subseteq A\}$$

Figure 22: Erosion Formula

The formula is read as follows: "The Erosion of set A by the kernel set B is equal to the translation of B to B_z by the vector z. z is an element of the square of the Euclidean Space and set A being a subset of the Euclidean space."

4.3.2. Dilation

Dilation is usually applied on binary images. However, there are some variations that are fit for application on gray-scale images. The basic idea of Erosion is to simultaneously **increase** the number of white pixels and decrease the number of black pixels in order to decrease holes.

$\oplus$ • Dilation

Figure 23: Dilation Operator

To fully understand the concept of erosion, the researcher has manually represented an image in the form of a matrix as shown in the following figure. The researcher wishes to highlight that 0s represent white pixels and 1s represent white pixels.

TEST Engineering & Management

March - April 2020
ISSN: 0193-4120 Page No. 202 - 215

$$\begin{pmatrix} 1 & 1 & 1 & 1 \\ 1 & 0 & 0 & 1 \\ 1 & 0 & 0 & 1 \\ 1 & 1 & 1 & 1 \end{pmatrix}$$

Figure 24: Original Image Matrix

The researcher has defined a 2 x 2 kernel which is shown in the following figure:

$$\begin{pmatrix} 1 & 1 \\ 1 & 1 \end{pmatrix}$$

Figure 25: Kernel 2 X 2 Matrix

This kernel is now slid over the image for probing. The basic logic behind this probe is to check if there is a perfect match between the kernel and the image. The result of the probe over each pixel arises to two (**2**) scenarios:

- **Some / Perfect Match:** One/all of the image pixel values match one/all of the kernel pixel values at the point where the kernel is being applied. The result of the probe will be 0 assigned to the image pixel.
- **No Match:** One or all the image pixel values do not match the all the kernel pixel values at the point where the kernel is being applied. The result of the probe will be 1 assigned to the image pixel.

The probing process will be carried out in the same way as erosion except that the result of the scenarios will be different. The final dilation matrix will be experiencing an increase in white pixels and a decrease in black pixel. In this case the dilation matrix will be the same as the original matrix as shown below:

$$\begin{pmatrix} 1 & 1 & 1 & 1 \\ 1 & 0 & 0 & 1 \\ 1 & 0 & 0 & 1 \\ 1 & 1 & 1 & 1 \end{pmatrix}$$

Figure 26: Final Image Matrix After Dilation

In a more mathematical way of representation, dilation is shown as a formula as shown below:

$$A \oplus B = \{z \in E \,|\, (B^s)_z \cap A \neq \varnothing\}$$

Figure 27: Erosion Formula

The formula is read as follows: "The Erosion of set A by the kernel set B is equal to the translation of B to the radial symmetry of B_z by the vector z. z is an element of the Euclidean Space.

The researcher wishes to add that Erosion and Dilation are actually considered the two (**2**) most basic mathematical morphology operators while the rest are a combination of erosion and dilation.

An example of applying dilation on a binary image is shown below:

[28] ***[29]***

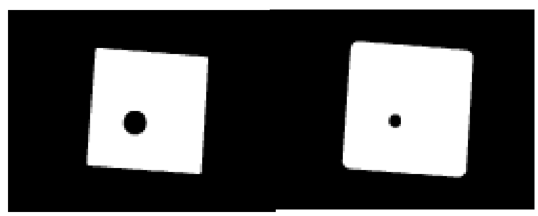

Figure 28: Original Image, Figure 29:Resulting Image After Applying Dilation

4.3.3. Opening

Opening operator is a derivative operator of erosion and dilation. When opening operator is applied on an image, the image firstly undergoes a binary erosion process succeeded by a dilation process by utilizing the same kernel for both binary operations.

$\bigcirc$ • Opening

Figure 30: Opening Operator

Opening operator follows the same objective of erosion by decreasing the white pixels and increasing the black pixels. The opening operator, however tends to be better than erosion by preserving the edges and the shape of the objects in the image.

In a more mathematical way of representation, opening is shown as a formula as shown in the following:

TEST Engineering & Management

March - April 2020
ISSN: 0193-4120 Page No. 202 - 215

$$A \circ B = (A \ominus B) \oplus B$$

Figure 31: Opening Formula

The formula is read as follows: "The Opening of set A by the kernel set B is equal to the erosion of A by B followed by a dilation of the resultant set by B.

An example of applying opening operator on a binary image is showcased in the following:

[32] ***[33]***

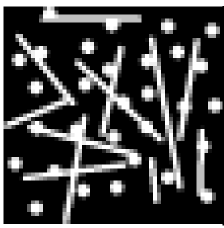

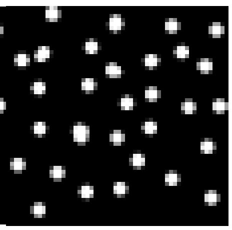

Figure 32: Original Image, Figure 33:Resulting Image After Applying Opening

4.3.3. Closing

Closing operator is a derivative operator of erosion and dilation. When opening operator is applied on an image, the image firstly undergoes a dilation process succeeded by an erosion process by using the same kernel for both binary operations.

Figure 34: Closing Operator

Closing operator follows the same objective of dilation by decreasing the black pixels and increasing the white pixels. The closing operator, however tends to be better than dilation by preserving the edges and the shape of the objects in the image.

In a more mathematical way of representation, closing is shown as a formula as shown in the following:

$$A \bullet B = (A \oplus B) \ominus B$$

Figure 35:Closing Formula

The formula is read as follows: "The Closing of set A by the kernel set B is equal to the dilation of A by B followed by an erosion of the resultant set by B.

An example of applying Closing operator on a binary image is showcased in the following:

[36] ***[37]***

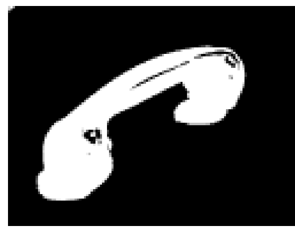

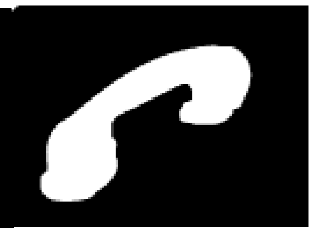

Figure 36: Original Image, Figure 37:Resulting Image After Applying Closing

4.4.Sobel Operator

The Sobel Operator is an image segmentation approach that emphasizes on edge detection. Sobel Operator works on colour images, grayscale images as well as on binary images. The Sobel Operator is preferred as it gives a detailed processed image consisting of edges.

The Sobel operator can be considered a mathematical morphology approach. It makes use of two (**2**) kernel matrices – one kernel being used for the y-axis while the other one for the x-axis.

To better understand how Sobel Operator works, the researcher has represented the pixels of an image in a matrix format as shown:

50	50	100	100
50	50	100	100
50	50	100	100
50	50	100	100

Figure 38: Original Image Matrix

The kernels defined for applying the Sobel Operator are shown in the following figure. The first kernel will be used for the x-axis while the second kernel will be used for the y-axis.

March - April 2020
ISSN: 0193-4120 Page No. 202 - 215

$$\begin{pmatrix} -1 & 0 & 1 \\ -2 & 0 & 2 \\ -1 & 0 & 1 \end{pmatrix}$$

Figure 39: Gx-Axis Kernel

$$\begin{pmatrix} -1 & -2 & -1 \\ 0 & 0 & 0 \\ 1 & 2 & 1 \end{pmatrix}$$

Figure 40:Gy-Axis Kernel

It can be seen that the middle column in the kernel of the x-axis and the middle row in the kernel of the y-axis have values on zero (**0**). Now, the researcher will use the x-axis kernel to probe the image:

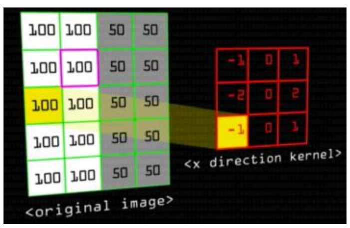

Figure 41: Applying Sobel Kernel On Image

The kernel is applied on the image with the purple square as the chosen pixel for probing. The values of the pixel intensities of the original image will be multiplied and added to the values of the kernel matrix of the right-hand side and the left-hand side as shown:

- Left-hand side: (-1 x 100) + (-2 x 100) + (-1 x 100) = -400;
- Right-hand side: (1 x 50) + (2 x 50) + (1 x 50) = 200;

The values of the sum of the right-hand side and the left-hand side are added. There will be three scenarios:

- A negative result is obtained meaning that there is a change in intensity. If a negative value is obtained, the pixel is changed to a black pixel of 0.
- A positive result is obtained meaning that there is a change in intensity. If a positive value is obtained, the pixel is changed to a white pixel of 1.
- If the result is zero, there is no change in pixel intensity and hence, no edge is found.

The values are added for the picture as shown:

(-400) + (200) = -200

Since it is a non-zero result, there is an edge found.

The same principle is applied for the kernel of the y-axis by multiplication of the top row and bottom of the kernel with the matching image pixel intensities and adding the values.

An example of applying Sobel Operator is shown below:

[42] ***[43]***

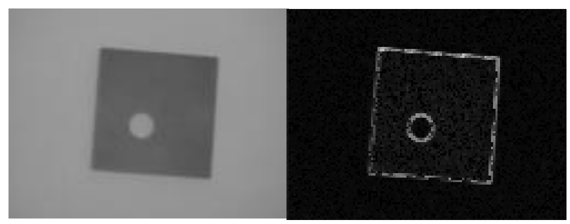

Figure 42:Original Image, Figure 43:Resulting Image After Applying Sobel Operator

4.5.Otsu's Algorithm

In Otsu's Thresholding algorithm, discovered by Noboyuki Otsu, a gray-scale representation of an image is assumed to be bimodal. This means that the pixels in an image are assumed to be divided into two (**2**) sets namely foreground pixels and background pixels. [20][21]

To understand the concept of Otsu's algorithm, the researcher has come up with a simpler way of explaining Otsu's algorithm as shown below:

First of all, allow the researcher to assume that there is a certain image:

March - April 2020
ISSN: 0193-4120 Page No. 202 - 215

Figure 44:Grayscale Representation Of Image

This image has been enhanced to remove noises so that the image contains even distribution of pixels. Below is an assumed histogram for the image:

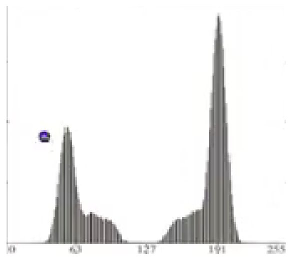

Figure 45:Assumed Histogram

There are two classes of pixels (two peaks/ or two modes). The first class of pixels is in the left mode and the second class of pixels is in the right mode.

According to the definition of a threshold, it acts as a benchmark for comparison. In this case, the threshold value is the value which is in the middle of the two modes. This is where Otsu's algorithm enters in action. Otsu's thresholding technique has been regarded by several researchers as one of the most powerful image segmentation algorithms. [20][21]

The main concept behind Otsu's algorithm is to search for that particular threshold value that optimizes the **weighted within class variance**. The weighted within class variance, also known as the intra-class variance, is the weighted sum of each of the pixel classes. [20][21]

$$\sigma_w^2(t) = q_1(t)\sigma_1^2(t) + q_2(t)\sigma_2^2(t)$$

Figure 46: Weighted Within Class Variance

From this above formula, it can be seen that $\mathbf{q_1}$and $\mathbf{q_2}$are the probabilities of the two-pixel clusters while $\sigma^2{}_1$ and $\sigma^2{}_2$ are their class probabilities.

The class probabilities are calculated using the formulae on the next page:

$$q_1(t) = \sum_{i=1}^{t} P(i) \quad q_2(t) = \sum_{i=t+1}^{I} P(i)$$

Figure 47:Classes Probabilities

In order to segment a certain image, we need to find that specific threshold (t) which will help to simultaneously keep the pixel classes as tight as possible and reduce the overlapping of the two clusters. Minimization of the within-class variance helps to keep the clusters as tight as possible. Therefore, all that a system needs to do is to iterate through the values of t [which is calculate the outcomes of t = 1, t = 2 ... t = 256] until the specific value of t is obtained which minimizes the value of $\sigma^2{}_w(t)$. [20][21]

Since the total variance(σ^2) is the sum of the within-class variance and the between class variance (also known as the inter-class variance) as shown in the formula below:

$$\sigma^2 = \underbrace{\sigma_w^2(t)}_{\substack{\text{Within-class,}\\ \text{from before}}} + \underbrace{q_1(t)[1-q_1(t)][\mu_1(t)-\mu_2(t)]^2}_{\text{Between-class, } \sigma_B^2(t)}$$

Figure 48:Total Variance

Due to the fact that the total is independent of t, Otsu showcases that decreasing the intra-class variance is the same as maximizing the inter-class variance.

$$\sigma^2{}_B(t) = \sigma^2 - \sigma^2{}_w(t)$$

In brief, Otsu's algorithm comprises of computing the probabilities of each intensity level, iterating through all the threshold values and choose the threshold value that maximizes the inter-class variance. [20][21]

March - April 2020
ISSN: 0193-4120 Page No. 202 - 215

5. Discussions and conclusion

In this paper, we have carried an extensive review on the state-of-the-art image processing techniques mostly used by researchers to automatically detect Diabetic Retinopathy. Those algorithms have been explained by the researchers in a simple and convenient manner such that readers are able to grasp a firm understanding of how to use those mentioned algorithms to compute digital images in the aim of developing more accurate diabetic retinopathy detection systems.

The systems that have been mentioned above has been developed for research purposes. Due to the inconsistent levels of accuracy that have been the challenge since the invent of such systems, most ophthalmologists are still using manual screening rather than automatic screening for such exudate detection. This paper contributes towards the aim of developing commercially used ocular imaging systems that shall heavily revolutionize the healthcare sectors of developing and developed countries as well as advancements in the field of developing smart hospitals.

References

[1] I. D. Federation, "Diabetic Retinopathy Barometer," 2018. [Online]. Available: https://www.idf.org/e-library/epidemiology-research/diabetes-atlas/92-diabetic-retinopathy-barometer.html.

[2] T. o. Islamabad, "Times of Islamabad," 14 November 2016. [Online]. Available: https://timesofislamabad.com/14-Nov-2016/diabetes-mother-of-all-diseases-experts.

[3] N. E. Institute, "Diabetic Retinopathy Defined," n.d.. [Online]. Available: https://nei.nih.gov/eyedata/diabetic.

[4] M. Clinic, "Diabetic Retinopathy," n.d.. [Online]. Available: https://www.mayoclinic.org/diseases-conditions/diabetic-retinopathy/symptoms-causes/syc-20371611.

[5] I. C. o. Ophthalmology, "Number of Ophthalmologists in Practice and Training Worldwide," n.d.. [Online]. Available: http://www.icoph.org/ophthalmologists-worldwide.html.

[6] A. Janus, "Poverty a leading cause of Type 2 diabetes, studies say," 21 November 2010. [Online]. Available: https://www.ctvnews.ca/poverty-a-leading-cause-of-type-2-diabetes-studies-say-1.576721.

[7] M. U. Saeed and J. D. Oleszczuk, "Advances in retinal imaging modalities: Challenges and opportunities," World Journal of Ophthalmology, vol. 6, no. 2, pp. 10-19, 12 May 2016.

[8] G. G. Gardner, T. H. W. D Keating and A. T. Elliott, "Automatic detection of diabetic retinopathy using an artificial neural network: a screening tool," British Journal of Ophthalmology, vol. 80, no. 11, pp. 940-944, 1996.

[9] C. Sinthanatothin, T. H. W. J. F. Boyce, h. L. Cook, E. Mensah, S. Lal and D. Usher, "Automatic Detection of diabetic retinopathy on digital fundus images," Diabetic Medicine, vol. 19, no. 22, pp. 105-112, 2002.

[10] A. Sopharak, B. Uyyanonvara, S. Barman and T. H. Williamson, "Automatic detection of diabetic retinopathy exudates from non-dilated retinal images using mathematical morphology methods," Computerized Medical Imaging and Graphics, vol. 32, no. 8, pp. 720-727, 2008.

[11] A. Sopharak, B. Uyyanonvara and S. Barman, "Automatic Exudate Detection from Non-dilated Diabetic Retinopathy Retinal Images Using Fuzzy C-means Clustering," Sensors, vol. 9, no. 3, pp. 2148-2161, 2009.

[12] J. A. Stark, "Adaptive Image Contrast Enhancement Using Generalizations of Histogram Equalization," IEEE TRANSACTIONS ON IMAGE PROCESSING, p. 8, May 2000.

[13] U. o. Utah, "Histograms," 2018. [Online]. Available: http://www.sci.utah.edu/~acoste/uou/Image/project1/Arthur_COSTE_Project_1_report.html. [Accessed June 21 2018].

[14] S. Gupta and Y. Kaur, "review of Different Local and Global Contrast Enhancement Techniques for a Digital Image.," International

March - April 2020
ISSN: 0193-4120 Page No. 202 - 215

Journal of Computer Applications, vol. 100, no. 18, p. 6, 18 August 2014.

[15] E. A. Haller, "Adaptive histogram equalization in GIS," Annals of the University of Craiova, vol. 38, no. 1, p. 104, 2011.

[16] S. S. B. Anu Namdeo, "A Review on Image Enhancement Techniques with its Advantages and Disadvantages," International Journal for Science and Advance Research in Technology, vol. 2, no. 5, p. 12, May 2016.

[17] S. Esakkirajan, T. Veerakumar, A. N. Subramanyam and C. H. PremChand, "Removal of High Density Salt and Pepper Noise Through Modified Decision Based Unsymmetric Trimmed Median Filter," IEEE SIignal Processing Letters, vol. 18, no. 5, p. 4, May 2011.

[18] Y. Zhu and C. Huang, "An Improved Median Filtering Algorithm for Image Noise Reduction," in International Conference on Solid State Devices and Materials Scence, Changzhou, 2012.

[19] R. Fisher, S. Perkins, A. Walker and E. Wolfart, "Median Filter," 2004. [Online]. Available: https://homepages.inf.ed.ac.uk/rbf/HIPR2/median.htm. [Accessed 23 June 2018].

[20] N. Otsu, "A Threshold Selection Method from Gray-Level Histogram," IEEE Transactions on Systems, Man and Cybernetics, vol. 9, January 1979.

[21] D. Liu and J. Yu, "Otsu Method and K-means," 2009 Ninth International Conference on Hybrid Intelligent Systems, no. 978-0-7695-3745-0, 9 September 2009.